

Elastic and optical properties of zinc-blende CrSb and its effective mass

Sahar Rezaee, Arash Boochani*, Masoud Majidiyan,
Atefeh Ghaderi, Shahram Solaymani,
Mosayeb Naseri

Received: 15 March 2013 / Revised: 28 May 2013 / Accepted: 23 January 2014 / Published online: 18 March 2014
© The Nonferrous Metals Society of China and Springer-Verlag Berlin Heidelberg 2014

Abstract The elastic, optical, and effective mass properties of CrSb in zinc-blende (ZB) phase were investigated. The calculations were carried out using the full-potential linearized augmented plane wave plus local orbital according to the density functional theory. The results of elastic calculations by generalized gradient approximation and local density approximation approximations indicate that ZB CrSb is a ductile material and its Debye temperature is rather low. Band structure and density of state calculations introduce the ZB CrSb as a half-metal with spin polarization of 100 %. In metal state, 16th and 17th bands cut off the Fermi level. Calculations study the effective mass, Fermi velocity, and Fermi surface at 16th and 17th bands. In continue, optical quantities such as dielectric function, energy loss function, and optical conductivity were investigated.

Keywords Half-metal; CrSb; Elastic properties; Optical properties

1 Introduction

Spintronic devices, which exploit the spin of electrons as well as their charge, have already yielded breakthrough in

information storage and hold the promise of doing the same for memory, microprocessors, and a host of other technologies [1–4]. In spintronic applications, the critical materials are ones containing atoms with large atomic magnetic moments ($I > \mu_B$, where μ_B is the Bohr magneton) and high Curie temperatures (above room temperature).

The “half-metal” term in studying the Cl_b -type Heusler alloys, NiMnSb, and PtMnSb was first introduced by De Groot et al. [5]. Half-metals are so named because one spin channel is metallic while the other is insulating. The polarization of the carriers is thus complete, contributed entirely by one spin channel at Fermi energy, E_F . This is in marked contrast to the usual ferromagnetic metals such as iron in which both spin channels contribute at E_F , resulting in substantially less than 100 % polarization.

Also, the half-metallic behavior is detected in some oxides such as CrO_2 [6] and magnetic (Fe_3O_4) [7]. Recently, many theoretical and experimental attempts have been done on the ZB compounds such as MAs and MSb (M is a transition-metal element) [8–16], which are compatible with III–V and II–VI semiconductors. Later Liu [17] theoretically predicted that the ZB CrSb phase is a robust half-metallic ferromagnetic with magnetic moment of $3 \mu_B$ per unit formula and its HM gap reaches 0.774 eV also persisting to be nonzero even when compressed by 21 %. According to the results, the ferromagnetic ZB phase of CrSb is about 1 eV higher in total energy than the anti ferromagnetic, NiAs phase; therefore, ZB CrSb should not exist as bulk crystal, but can be grown as thin film epitaxially on III–V semiconductors [12]. So a practical approach for stabilizing the CrSb compound in metastable ZB structure is the pseudomorphic growth of CrSb thin film on ZB semiconductors. The lattice parameter of ZB and NiAs-type structure for CrSb is calculated to be equal to 0.614 nm [17] and $a = 0.403$ nm and $c = 0.592$ nm,

S. Rezaee, A. Boochani*, M. Naseri
Department of Physics, College of Science,
Islamic Azad University, Kermanshah 6718997551, Iran
e-mail: arash_bch@yahoo.com

M. Majidiyan
Physics Department, Sabzevar Tarbiat Moallem University,
Sabzevar 9613152365, Iran

A. Ghaderi, S. Solaymani
Young Researchers and Elite Club, Islamic Azad University,
Kermanshah 6718997551, Iran

respectively [18]. Since the Half-metallic properties of ZB CrSb were already reported by others, we focus on those features of the bulk properties such as elastic, optical, and effective mass properties that have not been touched by others.

Here, after presenting computational method, the elastic constants and optical property results for ZB CrSb were investigated. Finally, the effective mass and Fermi velocity were investigated.

2 Computational method

The calculations reported in this work were carried out with WIEN2K program developed by Blaha et al. [19]. This program used the full-potential linearized augmented plane wave plus local orbitals [20] approach (FP-APW + LO) based on density functional theory. The exchange–correlation energy of electrons was described in the generalized gradient approximation (GGA) [21]. Also, in comparison, the local density approximation (LDA) [22] was used. In this method, the space was divided into an interstitial region (IR) and nonoverlapping (MT) spheres centered at the atomic sites. In IR region, the basis sets consist of a plane wave. Inside the MT spheres, the basis sets was explained by radial solutions of the one particle Schrödinger equation [23] (at fixed energy) and their energy derivatives multiplied by spherical harmonics. Basis functions, charge density, and potential were expanded inside MT spheres in combination with spherical harmonic functions with a cut-off $l_{\max} = 10$, and in Fourier series in the IR region. Moreover, a parameter $R_{\text{MT}}K_{\max} = 8$ was used to determine the matrix size (convergence), where K_{\max} was the plane wave cut-off and R_{MT} the smallest of all atomic sphere radii. For all atoms, R_{MT} was chosen as 2.1 a.u. The self-consistent calculations were considered to be converged only when the integrated charge differed per formula unit, $\int |\rho_n(\rho_{n-1})|dr$ between input charge density $[\rho_{n-1}(r)]$ and output charge density $[\rho_n(r)]$ which is less than 0.00001.

3 Results and discussion

3.1 Elastic properties

Crystals in cubic symmetry have only three distinct non-vanishing elastic constants, namely c_{11} , c_{12} and c_{44} . For calculating these values, the cubic unit cell is deformed using appropriate strain tensors to yield energy-strain relation. These data which are dependence to used

symmetry of the strain tensor, yield the specific elastic constant. In the present work, it was used the strain tensors and the strain-energy relations described in Ref. [18]. The calculation of c_{44} requires a relaxation of atoms' positions which significantly improves the obtained results, as can be seen from [24]. The calculated elastic constants are listed in Table 1. The bulk modulus B can be calculated from the elastic constants using the following equation:

$$B = (c_{11} + 2c_{12})/3 \quad (1)$$

which provides a useful internal consistency between various computational procedures. The mechanical stability of a crystal can be checked by means of the elastic constants which satisfies special restrictions. For cubic materials, the stability criteria are described via $B > 0$; $c_{11} - c_{12} > 0$ and $c_{44} > 0$. According to Table 1, whereas $c_{11} - c_{12} < 0$, $B < 0$, and $c_{44} > 0$ are predictable that ZB structure is meta-stable using GGA and LDA approximations.

The shear modulus G , Young modulus E , and Poisson's ratio ν for polycrystalline can be calculated from the elastic constants. The shear modulus, a measure of the directional bonding, is bounded by Reuss and Voigt's modules, G_{R} and G_{V} , which represent the lower and upper limits, respectively [25].

For cubic lattices these modules are given by:

$$G_{\text{R}} = \frac{5(c_{11} - c_{12})c_{44}}{[4c_{44} + 3(c_{11} - c_{12})]} \quad (2)$$

and

$$G_{\text{V}} = \frac{(c_{11} - c_{12} + 3c_{44})}{5} \quad (3)$$

and practically the Hill's arithmetic mean value is taken for G

$$G = \frac{1}{2}(G_{\text{R}} + G_{\text{V}}) \quad (4)$$

The bulk and shear modules are used to calculate E and the ν as follow:

$$E = \frac{9BG}{3B + G} \quad (5)$$

$$\nu = \frac{3B - E}{6B} \quad (6)$$

The calculated values of G , E , and ν for the ZB phase are listed in Table 1. The quotient of bulk to shear modulus (B/G) provides a simple empirical relationship between the plastic properties of materials and their elastic module. This quotient was introduced by Pugh, in which B represents the resistance to fracture and G is the resistance to plastic deformation. According to GGA and LDA approximations and as can be seen from Table 1, B and G are great and small, respectively.

Table 1 Elastic constants c_{xx} (GPa), shear modulus G (GPa), Young modulus E (GPa), Poisson's ratio ν , mean sound velocity v_m ($\text{m}\cdot\text{s}^{-1}$), and Debye temperature (K)

Parameters	c_{11} /GPa	c_{12} /GPa	c_{44} /GPa	G /GPa	B /GPa	E	ν	$v_m/(10^3 \text{ m}\cdot\text{s}^{-1})$	θ_D/K
GGA	34.61	49.02	58.25	4.97	44.21	14.38	0.445	2.26	56.69
LDA	46.55	47.58	13.03	3.12	47.23	9.16	0.467	1.80	69.88

A high value of this quotient points to the ductility of the materials, whereas a low value indicates its brittleness. The critical value of 1.75 separates ductile and brittle materials [26]. The high value of this quotient shows that the ZB structure is ductile. The (B/G) value for ZB CrSb is higher than 1.75 indicating that this structure is ductile material.

In the Debye model, the mean sound velocity v_m is connected to the longitudinal and transverse sound velocities, v_l and v_t , respectively, which can be obtained from the elastic moduli as follow:

$$v_l = \sqrt{\frac{(B + 4G/3)}{\rho}} \quad (7)$$

$$v_t = \sqrt{\frac{G}{\rho}} \quad (8)$$

and

$$v_m = \left[\frac{1}{3} \left(\frac{1}{v_l^3} + \frac{1}{v_t^3} \right) \right]^{-\frac{1}{3}} \quad (9)$$

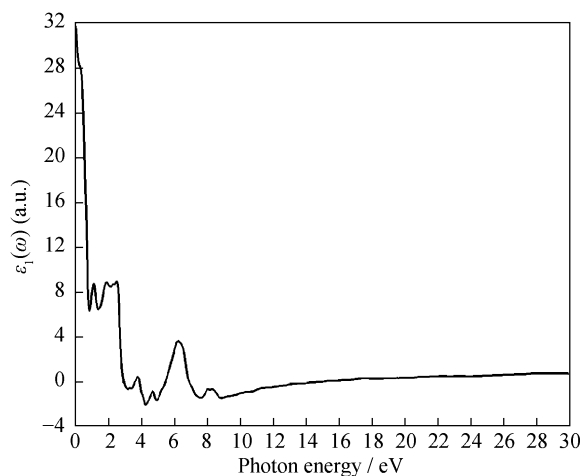
where ρ denotes the density of the material. Then the Debye temperature is given by [27]

$$\theta_D = \left(\frac{3N}{4\pi V_0} \right)^{\frac{1}{3}} \frac{h v_m}{k_B} \quad (10)$$

where N is the number of atom in the primitive unit cell, V_0 is the unit cell volume, also h and k_B are the Planck and Boltzmann's constants, respectively. The obtained Debye temperatures are listed in Table 1. By comparison of LDA and GGA approximations, it is clear that the calculated Debye temperature is very little. It is another tool indicating the ZB CrSb is meta-stable phase at mechanical view point.

3.2 Optical properties

The real part of dielectric function of CrSb compound is shown in Fig. 1. This compound is crystallized in cubic phase; therefore, only one direction was investigated. The value of static dielectric function or in other words, the function's value at low energies is obtained 32. This function is extremely decreased in the energy range of 0–1 eV because of its Half-metal property. Dielectric function is the reaction of matter with the electromagnetic

**Fig. 1** Real part of dielectric function of ZB CrSb

waves by showing the transmission, absorption, and loss of waves. It means that, wherever the real part of dielectric function is negative, the electromagnetic waves are weakened and absorption or reflection occurred.

For this compound, six roots in real part of dielectric function are observed at 2.99, 3.64, 3.92, 5.50, 6.94, and 14.61 eV, respectively. However, these roots are the required conditions for plasmonic frequencies. If the energy goes to waste in zero dielectric functions, the position of plasmonic frequency will be determined by that root.

Changes of energy loss function versus incident photon energy can be seen in Fig. 2, which shows that loss function's peaks are in energies of 3.64, 5.50, and 14.61 eV. These energies can be considered as compound's plasmonic energy. The width of forbidden band for propagating the electromagnetic waves increases by increasing the incident photon energy from 0.65 to 1.58 eV and finally to 7.67 eV.

According to free electron model the value of plasmonic energy is given by:

$$E_p = (n e^2 / \epsilon_0 m)^{0.5} \quad (11)$$

where m is the electron mass, n is density of free electrons per volume unit and ϵ_0 is vacuum permittivity.

The electron arrangements of compound's atoms are: Cr: [Ar] 3d⁵, 4s¹; Sb: [Kr] 4d¹⁰, 5s² 5p³

According to these arrangements, 3d orbital of Cr atom is filled and there is only one electron in 4s orbital. Therefore, if the single electron of 4s orbital of Cr atom

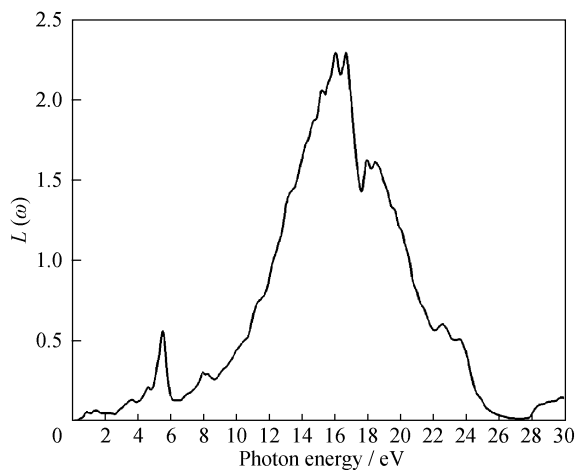


Fig. 2 Calculated energy loss function for ZB CrSb

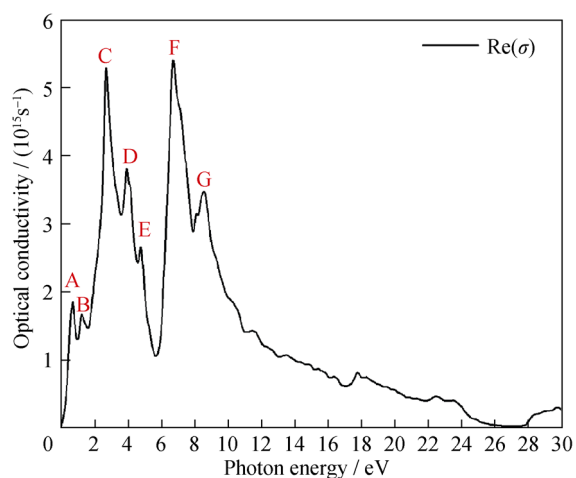


Fig. 3 Optical conductivity of ZB CrSb

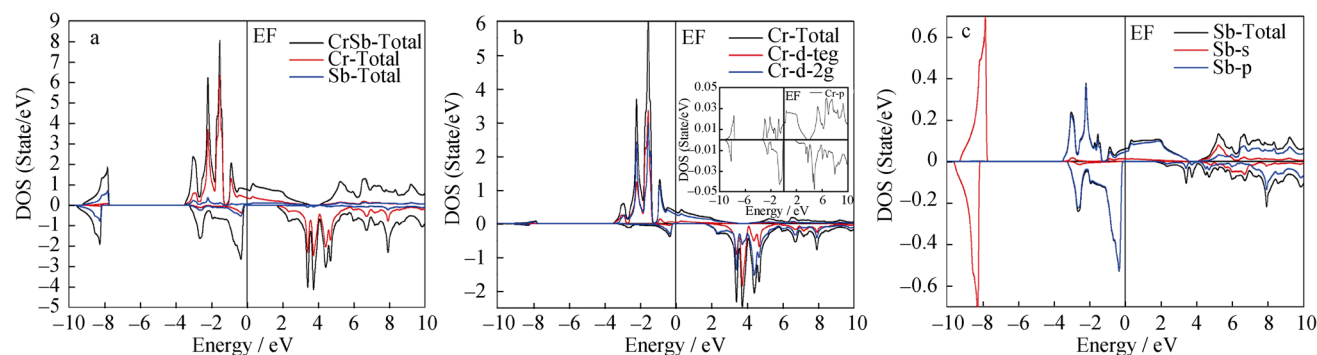


Fig. 4 DOS and PDOS diagrams for ZB CrSb at spin up and down by GGA + U approximation: **a** total DOS of CrSb, Cr and Sb atoms, **b** PDOS of Cr-d degeneracy orbitals, and **c** PDOS of Sb-s,p orbitals

is considered as free electron and last layer's electrons of Sb as free electrons, the amount of 6.01 eV will be obtained as value of plasmonic energy. On the other hand, if in Sb atom, the single electrons of 5p orbital and 4s in Cr atom are considered as free electrons, then the value of plasmonic energy will be obtained 4.91 eV. It can be seen that both energies are near the calculated energy (5.5 eV).

The optical conduction of compound is presented in Fig. 3. The compound's density of state (DOS) in spin up and down by GGA + U approximation was considered to plot Fig. 4 for investigating the peaks related to Fig. 3.

It appears that this compound behaves as a half-metal since it has metallic property for spin up and semiconductor property for spin down. In spin up under Fermi level, the majority of states are related to d orbital of Cr atom, but in spin down under Fermi level, the majority of states are related to both atoms with nearly the same ratio. Because of half-fill d orbital of Cr atom in CrSb compound, the DOS and PDOS diagrams were calculated using GGA + U approximation with $U = 0.25$ Ry (which was optimized).

Over the Fermi level, the states of Cr atoms are major. This portion for Sb atoms is related to widespread p orbital; however, Cr's p orbital are extended up to over Fermi level. From Fig. 3, the optical conduction peaks are located at energies of A (0.72 eV), B (1.26 eV), C (2.73 eV), D (3.96 eV), E (4.80 eV), F (6.73 eV), and G (8.55 eV).

Peak A is related to transmission from Cr-d-t_{2g}-up and Cr-d-e.g.-up to p-Sb which is located at Fermi level with more intensity in d-eg. Peak B is related to optical transmission in both up and down spins from Cr-d-t_{2g} and Cr-d-eg in energies from -1 eV to a little over Fermi level. In order to Peak C, these states are related to transmissions up to 1.5 eV over Fermi level which is the location of maximum Cr and Sb atoms' p orbital. For Peak D, transmissions from -1 eV to the end of p orbital are carried out by up and down spin states of Cr-d-teg and Cr-d-t_{2g}; whereas,

for Peak E, transmission at spin down state occurs from -2 eV to near the end of widespread of p orbital.

In partial density of state diagram for Cr and Sb in spin up state, there is a small singularity in p states at energy of 6.5 eV which provides the conditions for optical transmission of Peak F from Cr-d-eg and Cr-d-t_{2g} in up and down spin. According to the fact that Peak G occurs at high energies, it can be related to transmissions from state lower than Fermi level s-Sb to p-Sb and p-Cr at Fermi level.

Changes of CrSb compound's refractive index versus incident photon energy is shown in Fig. 5. The amount of static refractive index is 5.667. The same as real part of dielectric function previously discussed at refractive index quickly decreases. It is noteworthy that refractive index's peaks are in good accordance with optical conduction's peaks. And it shows that during optical transmissions, the refractive index increases and vice versa in regions with energy loss, especially in plasmonic energies, the refractive index is close to minimum values.

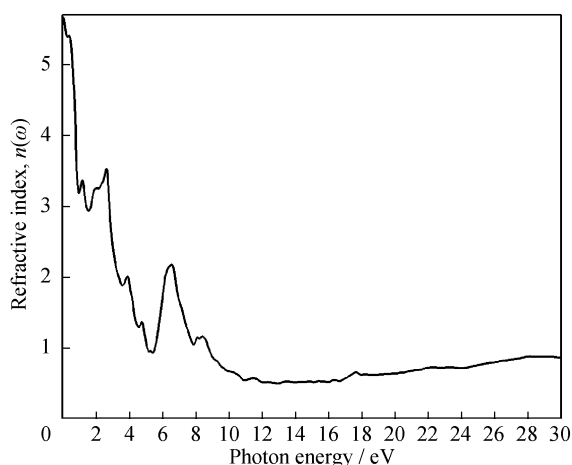


Fig. 5 Calculated refractive index for ZB CrSb

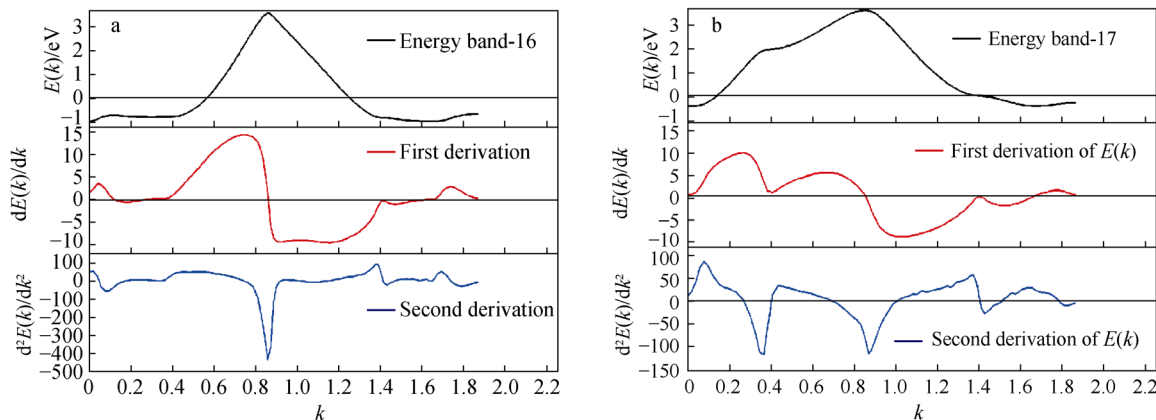


Fig. 6 Bands, first and second derivation band versus k vector for **a** 16th and **b** 17th bands

3.3 Effective mass and Fermi surface of CrSb

The “Effective mass tensor”, as follows is defined as:

$$[M^{-1}(k)]_{ij} = \pm \frac{1}{\hbar^2} \frac{\partial^2 E(k)}{\partial k_i \partial k_j} \quad (12)$$

where $-$ or $+$ sign, is determined according to the position of k . (If k is near maximum of band (holes) or minimum band (electrons)). Figure 6 shows energy band in terms of k for 16th and 17th bands, first and the second derivative. At the 16th band, second derivative of energy band to k strongly descends at the Γ point. Since, the Γ point is maximum for this band, then the second derivative minimum of 16th energy band determines hole's effective mass at the Γ point. For the 17th band, there are two clear minimums at the Γ and L points. The second derivative maximum is comparable with altitude of minimums. Based on the first derivative energy, we calculated the Fermi velocity. The Fermi wave length, Fermi velocity, and the effective mass of 16th and 17th bands are listed in Table 2. The 16th and 17th bands have two effective mass at Fermi level, and at 16th band, effective masses are negative whereas at 17th band are positive. The effective mass at 17th band is greater than effective mass at 16th band. By comparing the Fermi velocity, it is shown that the velocity at 16th band is grater than the Fermi velocity at 17th band.

Table 2 Effective mass per electron mass at Fermi level, length wave at Fermi level, Fermi velocity (Fermi level being interrupted by 16th band) at Bands 16 and 17

Band	$\frac{m_F^*}{m_e}$	λ_F/nm^{-1}	$v_F/(10^5 \text{ m}\cdot\text{s}^{-1})$
16th	0.525	0.593	6.502
	1.286	0.270	-6.950
17th	-0.667	0.555	5.602
	-1.420	0.235	-0.305

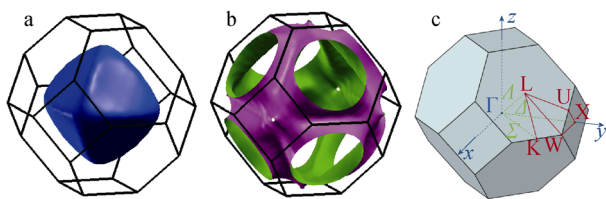


Fig. 7 Fermi surface of 16th band **a**, Fermi surface of 17th band **b**, and k path and high symmetry points **c**

The Fermi surface at 16th band is a closed octagon that completely lies inside the first Brillouin zone while Fermi surface at 17th band has necks on the Brillouin's planes. The neck mouths on the hexagonal plane are bigger than the neck mouth on the tetragonal planes inside the first Brillouin zone. In order to determine the distribution of valence electrons at the Fermi energy, the Fermi surface structures were calculated, whose 3D plots are shown in Fig. 7. These were obtained using the XCrysden code [28]. For CrSb, Band 16 is drawn as an electron sheet whereas Band 17 is drawn as an electron sheet. For Band 16, a voluminous form as an octahedron with rounded edges is seen around the zone center in Fig. 7. Band 17 exhibits a multiply-connected Fermi surface with hexagonal cavities for electron states at E_F centered on the L points. Also, six electron pockets are seen for Band 17 around X points.

4 Conclusion

The results given for elastic constants indicate that ZB CrSb is a meta-stable phase by GGA and LDA approximation, and it is also a ductile material. By comparing the LDA and GGA approximation, it is shown that the Debye temperature is calculated low.

Six roots in real part of dielectric function are observed for this compound at 2.99, 3.64, 3.92, 5.50, 6.94, and 14.61 eV, respectively. The loss function peaks are in energies of 3.64, 5.50, and 14.61 eV. These can be considered as compound's plasmonic energy. The width of forbidden band for propagating the electromagnetic waves increases by increasing the incident photon energy as in range from 0.65 to 1.58 eV and finally to 7.67 eV.

Band structure and DOS calculations show that ZB CrSb phase exhibits a half-metal behavior. The effective mass at 16th band is positive indicating the electron mobility, and at 17th band is negative indicating the hole's mobility.

The effective mass at 16th band is greater than the effective mass at 17th band. By comparing the Fermi velocity it is shown that the velocity at the 16th band is greater than the Fermi velocity at the 17th band. The Fermi surface at 16th band is a closed octagon that lies inside the first Brillouin zone. Band 17 exhibits a multiply-connected Fermi surface with hexagonal cavities for electron states at

E_F centered on the L points. Also, six electron pockets are seen for Band 17th around X points.

Acknowledgments This work was financially supported by Islamic Azad University (No. 67154281), Kermanshah Branch, Kermanshah, Iran. This work was jointly supported by the Simulation of Nano Physics Laboratory Center of Kermanshah Branch, Islamic Azad University.

References

- [1] Prinz GA. Magneto-electronics. *Science*. 1998;282(5394):1660.
- [2] Ball P. Meet the spin doctors. *Nature*. 2000;404:918.
- [3] Grünberg P. Layered magnetic structures: history, highlights, applications. *Phys Today*. 2001;54(5):31.
- [4] Wolf SA, Awschalom DD, Buhrman RA, Daughton JM, Molnár S, Roukes ML, Chtchelkanova AY, Treger DM. Spintronics: a spin-based electronics vision for the future. *Science*. 2001;294(5546):1488.
- [5] De Groot RA, Muller FM, Engen PG, Buschow KHJ. New class of materials: half-metallic ferromagnets. *Phys Rev Lett*. 1983;50(25):2024.
- [6] Schwarz K. CrO₂ predicted as a half-metallic ferromagnet. *J Phys F Met Phys*. 1986;16(9):L211.
- [7] Yanase A, Siratori K. Band structure in the high temperature phase of Fe₃O₄. *J Phys Soc Jpn*. 1984;53:312.
- [8] Flake T, Ramsteiner M, Kaganer VM, Jenichen B, Kastner M, Daweritz L, Ploog KH. Periodic elastic domains of coexisting phases in epitaxial MnAs films on GaAs. *Appl Phys Lett*. 2002;80(14):2523.
- [9] Ono K, Okabayashi J, Mizuguchi M, Oshima M, Fujimori A, Akinaga H. Fabrication, magnetic properties, and electronic structures of nanoscale zinc-blende MnAs dots. *J Appl Phys*. 2002;91(10):8088.
- [10] Akinaga H, Manago T, Shirai M. Material design of half-metallic zinc-blende CrAs and the synthesis by molecular-beam epitaxy. *Jpn J Appl Phys*. 2000;39:L1118.
- [11] Mizuguchi M, Akinaga H, Manago T, Ono K, Oshima M, Shirai M, Yuri M, Lin HJ, Hsieh HH, Chen CT. Epitaxial growth of zinc-blende CrAs/GaAs multilayer. *J Appl Phys*. 2002;91(10):7917.
- [12] Zhao JH, Matsukura F, Takamura K, Abe E, Chiba D, Ohno H. Room-temperature ferromagnetism in zinc blende CrSb grown by molecular-beam epitaxy. *Appl Phys Lett*. 2001;79(17):2776.
- [13] Radhakrishna P, Cable JW. Inelastic-neutron-scattering studies of spin-wave excitations in the pnictides MnSb and CrSb. *Phys Rev B*. 1996;54(17):11940.
- [14] Boochani A, Abolhasani MR, Ghoranneviss M, Elahi M. First principles study of half metallic properties of VSb surface and VSb/GaSb (001) interface. *Commun Theor Phys*. 2010;54(1):148.
- [15] Sartipi E, Hojabri A, Boochani A, Shakib MH. First principles study of half-metallic properties at MnSb/GaSb(001) interface. *Chin J Chem Phys*. 2011;24(2):155.
- [16] Shirai M. Possible half-metallic ferromagnetism in zinc blende CrSb and CrAs. *J Appl Phys*. 2003;93(10):6844.
- [17] Liu BG. Robust half-metallic ferromagnetism in zinc-blende CrSb. *Phys Rev B*. 2003;67(17):172411.
- [18] Pask JE, Yang LH, Fong CY, Pickett WE, Dag S. An Six low-strain zinc-blende half metals: ab initio investigation. *Phys Rev B*. 2003;67(22):224420.
- [19] Blaha P, Schwarz K, Sorantin P, Trickey SB. Full-potential, linearized augmented plane wave programs for crystalline systems. *Comput Phys Commun*. 1990;59(2):399.
- [20] Hohenberg P, Kohn W. Inhomogeneous electron gas. *Phys Rev*. 1964;136(3B):B864.

- [21] Perdew JP, Wang Y. Accurate and simple analytic representation of the electron-gas correlation energy. *Phys Rev B*. 1992;45(23):13244.
- [22] Langreth DC, Perdew JP. Theory of nonuniform electronic systems. I. Analysis of the gradient approximation and a generalization that works. *Phys Rev B*. 1980;21(12):5469.
- [23] Vanderbilt D. Soft self-consistent pseudopotentials in a generalized eigenvalue formalism. *Phys Rev B*. 1990;41(11):7892.
- [24] Mellouki A, Kalarasse L, Bennecer B, Kalarasse F. First principles calculations of the structural and elastic properties of the filled tetrahedral compounds LiCdX (X = N, P, As). *Comput Mater Sci*. 2008;42(4):579.
- [25] Mehl MJ, Klein BM, Papaconstantopoulos DA. Intermetallic Compounds: Principles and Practice. In: Westbrook JH, Fleisher RL, editors. *Principles*, vol. I. London: Wiley; 1995. 195.
- [26] Ravindran P, Fast L, Korzavyi PA, Johansson B, Will J, Eriksson O. Density functional theory for calculation of elastic properties of orthorhombic crystals: application to TiSi₂. *J Appl Phys*. 1998;84(9):4891.
- [27] Walecka JD. *Fundamental of Statistical Mechanics: Manuscript and Notes of Felix Bloch*. London: Imperial College Press/World Scientific; 2000. 72.
- [28] Kokalj A. XCrySDen—a new program for displaying crystalline structures and electron densities. *J Mol Graph Model*. 1999; 17(3–4):176.